Mon. Not. R. Astron. Soc. **391,** 369–382 (2008) doi:10.1111/j.1365-2966.2008.13896.x

Use of neural networks for the identification of new $z \geq 3.6$ QSOs from FIRST–SDSS DR5

R. Carballo,[1⋆] J. I. González-Serrano,[2] C. R. Benn[3] and F. Jiménez-Luján[2,4]

[1]*Dpto. de Matemática Aplicada y Ciencias de la Computación, Univ. de Cantabria, ETS Ingenieros de Caminos, Canales y Puertos, Avda de los Castros s/n, E-39005 Santander, Spain*
[2]*Instituto de Física de Cantabria (CSIC-Universidad de Cantabria), Avda de los Castros s/n, E-39005 Santander, Spain*
[3]*Isaac Newton Group, Apartado 321, E-38700 Santa Cruz de La Palma, Spain*
[4]*Dpto. de Física Moderna, Univ. de Cantabria, Avda de los Castros s/n, E-39005 Santander, Spain*

Accepted 2008 August 29. Received 2008 July 21; in original form 2008 March 19

ABSTRACT

We aim to obtain a complete sample of redshift $z \geq 3.6$ radio quasi-stellar objects (QSOs) from the Faint Images of the Radio Sky at Twenty cm survey (FIRST) sources ($S_{1.4\,\mathrm{GHz}} > 1$ mJy) having star-like counterparts in the Sloan Digital Sky Survey (SDSS) Data Release 5 (DR5) photometric survey ($r_{\mathrm{AB}} \leq 20.2$). Our starting sample of 8665 FIRST–DR5 pairs includes 4250 objects with spectra in DR5, 52 of these being $z \geq 3.6$ QSOs. We found that simple supervised neural networks, trained on the sources with DR5 spectra, and using optical photometry and radio data, are very effective for identifying high-z QSOs in a sample *without* spectra. For the sources with DR5 spectra the technique yields a completeness (fraction of actual high-z QSOs classified as such by the neural network) of 96 per cent, and an efficiency (fraction of objects selected by the neural network as high-z QSOs that actually are high-z QSOs) of 62 per cent. Applying the trained networks to the 4415 sources *without* DR5 spectra we found 58 $z \geq 3.6$ QSO candidates. We obtained spectra of 27 of them, and 17 are confirmed as high-z QSOs. Spectra of 13 additional candidates from the literature and from SDSS Data Release 6 (DR6) revealed seven more $z \geq 3.6$ QSOs, giving an overall efficiency of 60 per cent (24/40). None of the non-candidates with spectra from NASA/IPAC Extragalactic Database (NED) or DR6 is a $z \geq 3.6$ QSO, consistently with a high completeness. The initial sample of high-z QSOs is increased from 52 to 76 sources, i.e. by a factor of 1.46. From the new identifications and candidates we estimate an incompleteness of SDSS for the spectroscopic classification of FIRST $3.6 \leq z \leq 4.6$ QSOs of 15 per cent for $r \leq 20.2$.

Key words: methods: data analysis – surveys – galaxies: high-redshift – quasars: general – early Universe – radio continuum: galaxies.

1 INTRODUCTION

Homogeneous statistical samples of high-redshift quasi-stellar objects (QSOs) allow not only investigation of the QSO phenomenon itself, but also provide important information for a wide variety of studies. In particular, the luminosity function of high-redshift QSOs provides strong constraints on the theory of the accretion of matter on to supermassive black holes in the nuclei of galaxies. The increasing evidence for a relation between the formation of galaxy bulges and supermassive black holes (Kormendy & Richstone 1995; Magorrian et al. 1998) emphasizes the importance of understanding the role of QSO activity in the formation and evolution of galaxies. The luminosity function of QSOs is also essential to quantify their contribution to the X-ray background and the ultraviolet (UV) ionizing flux at high redshift. In addition, the absorption spectra of these QSOs reveal the state of the intergalactic medium at early epochs.

Although radio-loud (RL) QSOs are a small subset of the QSO population, samples of high-redshift RL QSOs benefit from higher completeness, due to the drastically reduced contamination by stars in samples of radio selected QSO candidates, compared to optically (colour) selected QSO candidates (Richards et al. 2006). Moreover, the connection between radio and optical activity, which still needs to be understood, requires a comparison between RL and radio-quiet QSO populations. Ivezic et al. (2004) provide conclusive evidence that the distribution of radio-to-optical flux ratio for QSOs, i.e. the radio loudness, is bimodal (the so-called QSO radio dichotomy), on the basis of accurate optical and radio measurements of a large sample of RL QSOs obtained from the Sloan Digital Sky Survey

⋆E-mail: carballor@unican.es

(SDSS; York et al. 2000) and the Faint Images of the Radio Sky at Twenty cm survey (FIRST; Becker, White & Helfand 1995). Many studies suggest that RL QSOs reside in more massive galaxies and harbour more massive central black holes than radio-quiet QSOs, but the point is still controversial (see references for and against these arguments at Cirasuolo et al. 2006). A recent study by Jiang et al. (2007) based on a QSO sample drawn from SDSS and FIRST shows that the fraction of RL QSOs decreases with increasing redshift and with decreasing optical luminosity.

We aim to obtain a homogeneous sample of high-redshift RL QSOs (z above $\sim$3.6) drawn from correlation of the FIRST catalogue ($S_{1.4\,\mathrm{GHz}} > 1.0$ mJy) with unresolved objects in the SDSS Data Release 5 (DR5; Adelman-McCarthy et al. 2007). The area of overlap between FIRST and the DR5 imaging survey is $\sim$7391 deg^2 and the number of selected FIRST–SDSS matches is 8665 (Section 2). SDSS provides (i) *ugriz* photometry, which is a powerful tool for separating high-z QSOs from other populations (e.g. stars, QSOs with z below $\sim$3.6 or unresolved low-z galaxies); (ii) morphological classification, essential for distinguishing between high-z QSOs and galaxies or resolved low-z active galactic nuclei (AGN) and (iii) spectroscopy of many of our candidates (4250), selected as spectroscopic targets by SDSS DR5. Since SDSS spectroscopic observations necessarily lag the imaging, the total DR5 spectroscopic area is lower, with $\sim$5553 deg^2 included in the overlap with FIRST. Most of the candidates with available spectroscopy were classified by SDSS as QSOs, i.e. have a secure detection of a high-excitation emission line with full width at half-maximum (FWHM) $\geq$1000 km s^{-1}. The rest are galaxies, stars and objects of 'unknown' class. 52 DR5 sources were spectroscopically classified as $z \geq 3.6$ QSOs (Table 1).

Our approach to obtaining a high-z QSO sample was to extend the existing sample of 52 FIRST–DR5 high-z QSOs by applying automated learning techniques, specifically neural networks (NNs), to the 8665 FIRST–SDSS DR5 photometric matches. NNs have been shown to be powerful tools for both classification and regression tasks, in many fields of astronomy, and have subsequently been applied to predict object classes and/or astrophysical parameters. Fields where NNs have been applied include classification of stellar spectra (Bailer-Jones, Irwin & von Hippel 1998), morphological star/galaxy separation (e.g. Bertin & Arnouts 1996), morphological classification, spectral typing and/or photometric redshifts of galaxies (Folkes, Lahav & Maddox 1996; Lahav et al. 1996; Firth, Lahav & Somerville 2003; Collister & Lahav 2004, this paper reports the popular photometric redshift code ANNZ; Ball et al. 2004), QSO identification and/or QSO photometric redshifts (Carballo et al. 2004; Claeskens et al. 2006) and cross-matching of astronomical catalogues (Rohde et al. 2005).

QSO selection and estimation of QSO photometric redshifts are of prime importance for the SDSS project. Various studies address the problem using different machine learning approaches. Richards et al. (2004) applied a probability density analysis based on kernel density estimation of the colour distribution of stars and spectroscopically confirmed QSOs in SDSS Data Release 1 (DR1), to classify, as stars or QSOs, a catalogue of over 10^5 unresolved, $g \leq 21$ mag, UV-excess ($u - g \leq 1$) QSO candidates. The resulting efficiency and completeness (the latter evaluated for $g \leq 19.5$) for the selection of QSOs in the candidate sample was estimated to be around 95 per cent up to $z \simeq 2.4$–3.0, the redshift limit mainly arising from the restriction of the catalogue to UV-excess objects.

Suchkov, Hanisch & Margon (2005) applied the oblique decision tree classifier Class X to classify SDSS Data Release 2 (DR2) photometric objects into 25 classes (stars, red stars, 10 redshift bins for galaxies and 13 for AGN) using colour information and morphology (attributes 'resolved' or 'unresolved') from SDSS. For each of the 12 redshift bins for AGN with $\Delta z = 0.2$ and covering $0 \leq z \leq 2.4$, the completeness obtained for the test sample is in the range from 43 to 81 per cent, with an average 63 per cent. For the high-redshift bin, in the range $z = 2.4$–6.0, the completeness drops to 14 per cent, the remaining high-z AGN being classified as stars (47 per cent) or as AGN in the adjacent redshift bin $2.2 \leq z \leq 2.4$ (39 per cent). This result illustrates the difficulty in separating high-z QSOs from other classes. The efficiency or fraction of true high-z QSOs among the sources classified in the AGN high-z bin was $\sim$75 per cent.

Ball et al. (2006) applied decision trees, trained on the SDSS Data Release 3 (DR3) objects with available spectroscopy, to classify all photometric objects ($>10^8$) in SDSS DR3 in one of the three categories of star, galaxy or nsng (neither star nor galaxy), the latter including QSOs and 'unknown'. A blind test on the 2dF QSO Redshift Survey (2QZ; Crom et al. 2004), using the 8739 QSOs matching 2QZ and SDSS DR3, yielded 95 per cent completeness and 87 per cent efficiency. The authors do not discuss how the performance depends on redshift.

Bazell, Miller & SubbaRao (2006) use a semisupervised mixture model approach to analyse 10 000 objects spectroscopically classified in SDSS Data Release 4 (DR4) in the categories of stars, late-type stars, galaxies and QSOs with $z \leq 3$ and unknown, using as input data for the modelling SDSS colours and the spectroscopic class. Since the aim was to investigate the existence of possible new object types among the class of 'unknown' as well as subclasses among the remaining classes, 90 per cent of the sources in the categories of stars, late-type stars, galaxies and QSOs were also treated as unknown during the modelling. The best model includes 16 components, two of them of the non-pre-defined type, and one of the latter captures a region of the $u - g$ versus $g - r$ colour–colour diagram ($2 \leq u - g \leq 5, 0.5 \leq g - r \leq 1.5$) within the location of high-z QSOs in Richards et al. (2002), but intentionally rejected in the QSO selection by Richards et al. (2004) because of the high density of stellar contaminants in that region.

Gao, Zhang and Zhao (2008) compare the performance of k-dimensional trees and support vector machines in the separation between stars and QSOs, using a sample of stars and QSOs spectroscopically classified in SDSS DR5 and having a counterpart at the Two-Micron All Sky Survey (2MASS; Cutri et al. 2003). Both techniques yield a global efficiency and completeness as large as 97 per cent for $0 \leq z \leq 2.5$. However, again the accuracy drops significantly for $z > 2.5$.

Our work deals with the selection of high-z QSOs from SDSS–FIRST matches. As stated before, our restriction to radio detected sources drastically reduces the contamination by stars, enabling us to obtain classification accuracies at these redshifts better than those obtained in more general studies aimed at the selection of the whole population of QSOs, regardless of radio detection. The paper is structured as follows. The sample of FIRST–DR5 matches is presented in Section 2. In Section 3 we explore the performance of supervised NNs to separate high-z QSOs from the remaining spectral classes in the sample of 4250 sources with DR5 spectra, using multiband optical photometry and radio data. In Sections 4.1 and 4.2, we apply the trained NNs to the sample of 4415 sources without DR5 spectra, identifying 58 high-z QSO candidates. In Section 4.3 we check the reliability of this identification via comparison with spectra from the NASA/IPAC Extragalactic Database (NED), SDSS Data Release 6 (DR6) and follow-up spectroscopy with the William

Table 1. SDSS classification of the 4248 FIRST–DR5 matches having SDSS spectra.

Spectral type	Number
QSO $z < 3.6$	3754
QSO $z \geq 3.6$	52
Early-type star	133
Late-type star	97
Galaxy	59
Unknown	153
Total	4248

Herschel Telescope (WHT). The discussion and conclusions are presented in Section 5.

2 SELECTION OF THE SAMPLE

As an initial sample we selected *all* FIRST sources with an unresolved object in the PhotoPrimary[1] view of the SDSS DR5 Catalog Archive Server (CAS), within 1.5 arcsec of the radio position, with dereddened point spread function (PSF) magnitude $15 \leq r_{\rm AB} < 20.2$ and 'clean' photometry (i.e. rejecting objects with magnitude errors >0.2 in all five bands *ugriz*, or flagged as 'BRIGHT', 'SATURATED', 'EDGE', 'BLENDED' or 'CHILD'). We selected the *r* band because QSOs with redshifts $3.6 \leq z \leq 4.5$ are expected to have an enhanced emission at this band, due to the Lyα emission line falling within the covered spectral range. Vigotti et al. (2003) estimated that more than 99 per cent of FIRST-APM quasars with $3.8 \leq z \leq 4.5$, $E \leq 18.8$ and $S_{1.4\,\rm GHz} > 1.0$ mJy fall within 1.5 arcsec of the POSS I positions, and this matching radius was adopted for this work. In total 8665 FIRST sources fulfil the above requirements. Because of the exclusion of 'CHILD' objects (objects which are the product of deblending a blended object), in all cases there is *one* optical object per radio source. The corrections for Galactic extinction, derived from Schlegel, Finkbeiner & Davis (1998), were taken from SDSS. 4250 of the sources (49 per cent of the sample) have DR5 spectra (specifically, they are included in the SpecObj[2] view of the DR5 CAS). In fact, the magnitude limit $r = 20.2$ was set to ensure an approximately similar fraction of sources with and without spectra at DR5. The distribution of SDSS spectral types and redshifts for the objects with DR5 spectra, as quoted in SpecObj, are given in Table 1. The redshift distribution of the QSOs is shown in Fig. 1.

The redshifts of the QSOs with $z \geq 3.6$ were checked by visual inspection of the DR5 spectra. For two of them, SDSS 130941.36+112540.1 and SDSS 153420.23+413007.5, we found the redshifts provided by the SDSS pipelines to be likely incorrect, and subsequently the QSOs were identified in the SDSS DR5 Quasar Catalog (DR5Q; Schneider et al. 2007) with revised redshifts $z = 1.362$ and 1.400, respectively. These two QSOs were not considered further and are not included in Table 1 and Fig. 1. On the one hand the revised values were published after we had already trained the NNs with the objects in Table 1 and carried out most of the follow up observations of the selected candidates. On the other,

[1] Best SDSS observation of the object, and the object is located within the imaging survey area which has been finished to date. See http://cas.sdss.org/astrodr5/en/help/docs/tabledesc.asp

[2] This implies that the object was selected for spectroscopy as an SDSS science object, and that the spectrum was taken on a main survey plate. See http://cas.sdss.org/astrodr5/en/help/docs/tabledesc.asp

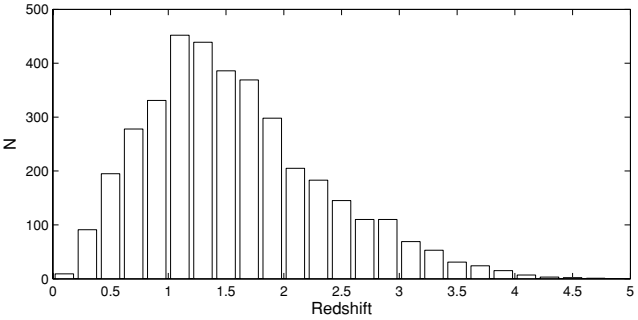

Figure 1. Redshift distribution of the 3806 FIRST QSOs with DR5 spectra.

having been misidentified as high-z QSOs in DR5 (redshift confidences 0.59 and 0.71, respectively), their exclusion from the training sample, used for the learning, seems reasonable. Since our aim is to obtain a high completeness for high-z QSOs, non-high-z sources whose spectra can be confused with those of high-z QSOs should be preferably removed from the training sample, since their inclusion could hinder the selection of the high-z QSOs whose spectra they resemble. We note that the redshift for SDSS 153420.23+413007.5 at DR6 has been updated to the high-confidence manual value $z = 1.400$, but for SDSS 130941.36+112540.1 the redshift obtained with the spectroscopic pipelines, $z = 4.395$ (confidence 0.55), has been maintained at DR6.

The spectral types and redshifts of the remaining 4196 sources in Table 1, most of them QSOs at $z < 3.6$, were taken directly from DR5, since we did not expect among them any $z \geq 3.6$ QSO with an identification as reliable as that found for the 52 high-z QSOs. A visual examination of the DR5 spectra of 225 of these sources [the first 125 $z < 3.6$ QSOs, 25 early-type stars, 25 late-type stars, 25 galaxies and 25 'unknown', in order of increasing right ascension (RA)] yielded no identification as a likely $z \geq 3.6$ QSO. Moreover, since our approach for the automated selection of high-z QSOs groups the remaining spectral types as a single class (see Section 3), revisions from DR5 such as shifts in redshift below this limit or changes between the non-high-z QSO categories would not affect the results.

The fraction of QSOs with $z \geq 3.6$ is 1.37 per cent (52/3806) and they are listed in Table 2. All these QSOs are included in DR5Q and only one of them, SDSS 141209.96+062406.8, with a deep and wide absorption feature bluewards of the Lyα emission line and starting at the Lyα line, has a revised redshift at DR5Q, $z = 4.467$ versus $z = 4.421$ at DR5. DR5Q provides interesting complementary information for these QSOs and for the remaining ones in Table 1, including i band absolute magnitudes, $g - i$ 'differential colour' with respect to the typical value for the QSO redshift, and matches to *ROSAT* All-Sky Survey (RASS; Voges et al. 1999, 2000) and 2MASS when available.

The FIRST–SDSS sample was obtained using a simple one-to-one match between radio and optical sources (within a 1.5-arcsec radius), therefore missing the class of double-lobe QSOs without detected radio cores. Using the statistics found by de Vries, Becker & White (2006, their table 2) for a sample of 5515 FIRST–SDSS QSOs with radio morphological information within 450 arcsec, the fraction of FIRST–SDSS double-lobe QSOs with undetected cores with respect to the total FIRST–SDSS QSO sample is 3.7 per cent. Since the starting samples of SDSS QSOs in de Vries et al. (2006) and in this work obey similar SDSS selection criteria, the last value is a good estimate of the incompleteness of the QSO samples in our work due to the exclusion of lobe-dominated QSOs.

Table 2. FIRST–DR5 sources with SDSS spectra, and classified by SDSS as $z \geq 3.6$ QSOs.

RA (J2000) (1)	Dec. (J2000) (2)	r_{AB} (3)	$S_{1.4\,GHz}$ (mJy) (4)	Redshift (5)	NN output y_{med} (6)	Previous samples (7)	Notes (8)
01 53 39.61	−00 11 05.0	18.82	4.75	4.194	1.00		
03 00 25.22	00 32 24.2	19.66	7.56	4.201	1.00		
07 51 13.05	31 20 37.9	19.75	5.60	3.761	0.11		abs
07 51 22.35	45 23 34.2	20.20	1.13	3.608	0.89		
08 10 09.95	38 47 57.0	19.62	27.16	3.946	0.29		
08 38 08.46	53 48 09.8	19.94	8.42	3.610	1.00		
08 39 46.22	51 12 02.8	19.33	41.64	4.390	1.00	1, 2	
08 40 44.18	34 11 01.6	19.79	13.59	3.889	1.00		
08 52 57.12	24 31 03.1	19.47	159.58	3.617	0.33		
09 18 24.38	06 36 53.3	19.77	26.50	4.192	0.84	2	abs
09 37 14.49	08 28 58.5	18.59	3.17	3.700	0.53		
09 40 03.02	51 16 02.7	19.99	13.91	3.601	0.03	3	
10 00 12.26	10 21 51.8	19.54	21.93	3.638	0.86		
10 17 47.75	34 27 37.8	20.00	2.63	3.691	0.91		
10 30 55.95	43 20 37.7	19.84	37.82	3.700	0.75		
10 34 46.54	11 02 14.5	18.80	1.09	4.266	0.70		
10 51 21.36	61 20 38.0	18.90	6.64	3.689	0.93		
10 57 56.28	45 55 53.0	17.44	1.38	4.137	1.00	1, 2, 3	
11 10 55.21	43 05 10.0	18.59	1.21	3.821	0.81	3	
11 17 01.89	13 11 15.4	18.28	28.99	3.624	0.14		
11 17 36.33	44 56 55.6	20.03	25.08	3.853	1.00		
11 25 30.48	57 57 22.7	19.41	2.99	3.685	0.70		abs
11 27 49.45	05 11 40.6	19.13	2.71	3.711	0.12		abs
11 29 38.73	13 12 32.2	18.77	1.33	3.607	0.21		
11 33 30.91	38 06 38.1	19.71	0.87	3.631	0.80		
11 50 45.61	42 40 01.1	19.87	1.51	3.894	0.54		
12 04 47.15	33 09 38.7	19.24	0.92	3.616	0.56		BAL
12 31 42.17	38 16 58.9	20.18	24.04	4.138	0.99		
12 40 54.91	54 36 52.2	19.74	15.09	3.938	1.00	3	
12 42 09.81	37 20 05.6	19.34	662.38	3.819	0.97		
12 46 58.83	12 08 54.7	20.00	1.44	3.805	1.00		BAL
12 49 43.67	15 27 07.0	19.31	2.01	3.995	0.89		
13 00 02.16	01 18 23.0	19.78	2.52	4.614	0.90		
13 03 48.94	00 20 10.4	18.90	0.99	3.647	0.99		BAL
13 07 38.83	15 07 52.1	19.70	3.89	4.082	0.94		
13 15 36.57	48 56 29.1	19.77	10.86	3.618	0.96		
13 25 12.49	11 23 29.7	19.33	71.05	4.409	1.00	2	
13 54 06.89	−02 06 03.2	19.18	719.48	3.715	0.67		
13 55 54.55	45 04 21.0	19.34	2.07	4.095	1.00		
14 08 50.91	02 05 22.7	19.07	1.18	4.008	0.06		abs
14 12 09.96	06 24 06.8	20.17	43.47	4.467[a]	0.90		abs
14 22 09.70	46 59 32.5	19.70	11.03	3.798	1.00		
14 23 26.48	39 12 26.2	20.15	6.52	3.921	1.00		
14 35 33.77	54 35 59.3	20.05	95.78	3.810	0.90		
14 45 42.75	49 02 48.9	17.32	3.18	3.876	0.99		
14 46 43.36	60 27 14.3	19.79	1.81	3.777	1.00		
15 03 28.88	04 19 49.0	17.96	124.97	3.664	0.84		
15 06 43.81	53 31 34.3	18.94	14.63	3.790	0.32	3	abs
16 17 16.49	25 02 08.1	19.99	2.35	3.943	0.98		BAL
16 19 33.65	30 21 15.1	19.52	4.19	3.794	0.92	3	
16 39 50.52	43 40 03.7	17.96	25.23	3.990	0.20	1, 2, 3	abs
16 43 26.24	41 03 43.5	20.10	65.01	3.873	1.00		

The columns give the following: (1, 2) SDSS coordinates; (3) SDSS dereddened PSF r_{AB} magnitude; (4) FIRST total radio flux density; (5) SDSS redshift ([a] = revised redshift from DR5Q, see Section 2); (6) NN output (see Section 4.2); (7) labels 1, 2 and 3 indicate QSOs included in the samples of Benn et al. (2002), Holt et al. (2004) and Carballo et al. (2006), respectively; (8) BAL – broad absorption line QSO; abs – the Lyα line appears to be self-absorbed.

3 SEPARABILITY OF HIGH-REDSHIFT QSOS WITH A NEURAL NETWORK

Only 52 of the 4248 sources with DR5 spectra are classified as $z \geq 3.6$ QSOs (Table 1). Our goal is to train a classifier to recognize high-z QSOs among the 4415 objects *without* SDSS spectra, i.e. the 'unlabelled' sources, after learning the class properties from the 4248 objects *with* spectra, i.e. the 'labelled' sources. The adopted procedure was to consider a two-class problem, with high-z QSOs as one class and the remaining types as the other. Since the training uses objects whose class is known, the learning is said to be 'supervised'.

Previous selections of high-z RL QSOs as FIRST sources with optical counterparts on POSS-APM revealed an abrupt change in $O - E$ colour with redshift at $\sim$3.6, the latter allowing efficient separation of high-z QSOs from the QSO population as a whole (Benn et al. 2002; Vigotti et al. 2003; Carballo et al. 2006). We therefore took this redshift as an initial threshold for high-z QSOs, although we explored redshifts below $z = 3.6$ to find the optimal value for the optical bands used in this work.

The learning algorithm applied was a feed-forward NN (Bishop 1995) with a layer for the input parameters, i.e. the data, and an output layer with a single variable y, set during training to 1 for high-z QSOs and 0 for the remaining types. Output y for object i is given by

$$y^i = f(a^i) = \frac{1}{1 + \mathrm{e}^{-a^i}},$$
$$\text{with} \quad a^i = w_0 + \sum_{j=1}^{d} w_j \, x_j^i,$$

where $(x_1, x_2, \ldots, x_d)$ are the inputs, a is a linear function of the inputs and f is the non-linear function known as a logistic sigmoid, with outputs in the range (0, 1). This NN model is known as logistic linear discriminant. w_0 and $(w_1, w_2, \ldots, w_d)$, called bias and weights respectively, are the parameters fitted during training. The adopted error function was the mean of the squared errors of the outputs:

$$\mathrm{mse} = \frac{1}{m} \sum_{i=1}^{m} (y^i - t^i)^2,$$

where m is the number of objects for the training and t is the desired value of output y or target value. The optimal parameters for the net, i.e. those minimizing the error, were obtained using the Levenberg–Marquardt algorithm, available in the MATLAB Neural Network Toolbox (http://www.matchworkds.com/). The Levenberg–Marquardt algorithm appears to be the fastest method for training moderate-sized NNs (Hagan & Menhaj 1994), and its efficient implementation in MATLAB further improves its performance.

Table 3. Combinations (A–H) of optical and radio data used as input variables to the NN.

	A	B	C	D	E	F	G	H
r magnitude	×	×	×	×	×	×	×	×
$u - g$	×	×	×	×	×	×	×	×
$g - r$	×	×	×	×	×	×	×	×
$r - i$	×	×	×	×	×	×	×	×
$i - z$	×	×	×	×	×	×	×	×
Rad–opt separation		×			×	×		×
$\log_{10}[S_{\mathrm{total}}(1.4\,\mathrm{GHz})]$			×		×		×	×
$\log_{10}(S_{\mathrm{total}}/S_{\mathrm{peak}})$				×		×	×	×

As input data we tried various combinations (A–H) of variables shown in Table 3. A pre-processing was performed normalizing each variable to the range $(-1, 1)$. For this step the total sample was used (unlabelled sources included) since the inputs for the new objects presented to the net need to have the same normalization as the data used in the learning process. The output values, $0 \leq y \leq 1$, give the degree of similarity with the class of high-z QSOs. Objects with y exceeding a given threshold y_c would be classified as high-z QSO candidates.

The quality of an NN for classification is evaluated in terms of its efficiency, *eff*, and completeness, *comp*. Efficiency is the fraction of sources with $y \geq y_c$ that actually are high-z QSOs. Completeness is the fraction of actual high-z QSOs with $y \geq y_c$. A good separation between two classes will show efficiency increasing and completeness decreasing as y_c increases. Since our purpose is to build a sample appropriate for statistical analysis, priority is given to completeness, accepting low y_c values at the cost of lower efficiency.

The classifier has to be empirically tested using a set of objects not used for the learning. Because of the small number of high-z QSOs, the training and test samples were separated adopting the partition method known as 'leave-one-out', repeatedly dividing the data set of m instances into a training set of size $m - 1$ and a test set of size 1, in all possible ways. This procedure yielded m classifiers, one per test object. Since the m objects (4248) are used for testing, a good estimate of the performance can be obtained.

The efficiency and completeness as a function of y_c for each of the eight sets of input variables is shown in Fig. 2. For all sets of features the expected trend between *eff* and *comp* is present, and classifiers are found yielding *comp* $\geq$90 per cent and *eff* $\geq$60 per cent for particular y_c values. Among these sets of inputs, B and E gave the maximum completeness, $\sim$96 per cent, both yielding $\sim$62 per cent efficiency. B was selected as the best classifier since it uses a smaller number of input variables. In total, 81 sources have $y \geq 0.1$ for this set, of which 50 are QSOs with $z \geq 3.6$, yielding completeness $50/52 = 96 \pm 14$ per cent and efficiency $50/81 = 62 \pm 9$ per cent for $y \geq 0.1$. The 31 contaminants include one star, two galaxies and 28 $z < 3.6$ QSOs. The redshift distribution of the latter is shown in Fig. 3. 19 of the QSOs, i.e. a fraction $19/31 = 61 \pm 14$ per cent of the contaminants, have redshifts $3.2 \leq z < 3.6$, very close to the selected threshold.

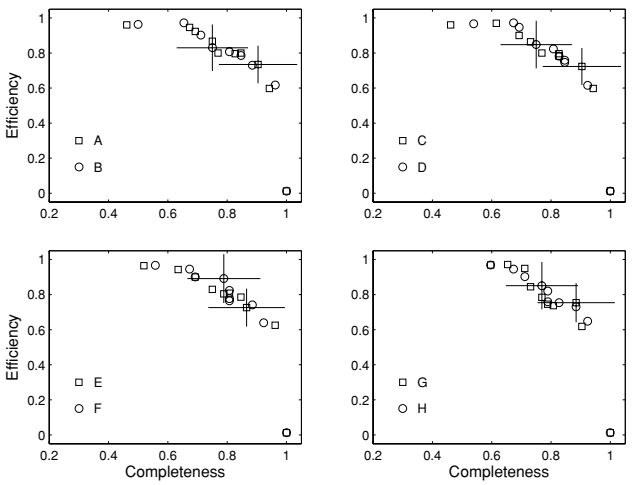

Figure 2. Efficiency versus completeness of the NN search for high-z QSOs, for y_c values 0, 0.1, 0.2, 0.3, 0.4, 0.5, 0.6, 0.7, 0.8, 0.9 (right to left) and the eight sets of input variables A–H. The adopted redshift cut for high-z QSOs was $z = 3.6$. A sample Poisson error bar is plotted for each set.

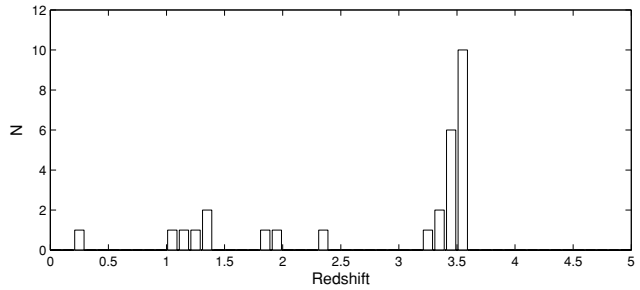

Figure 3. Redshift distribution for the 28 $z < 3.6$ QSOs with $y \geq 0.1$ (i.e. the contaminants), using the best-performing set of inputs, B.

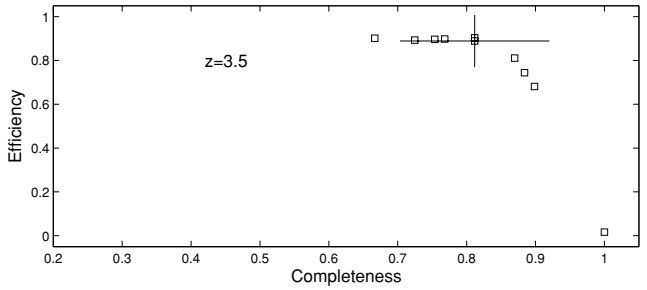

Figure 4. Similar to Fig. 2, but using the set of inputs B and with $z_{\rm cut} = 3.5$. The number of QSOs with higher redshift than this is 69.

Using a redshift cut $z_{\rm cut} = 3.5$ and the set of inputs B we found $comp = 90 \pm 11$ per cent and $eff = 68 \pm 9$ per cent for $y_{\rm c} = 0.1$ (Fig. 4). Since completeness was prioritized we kept $z_{\rm cut} = 3.6$, yielding completeness ∼96 per cent.

The inputs used for the learning were basically the SDSS colours, which are known to be correlated, especially for QSOs (Weinstein et al. 2004). This means that we could have applied some pre-processing algorithms to reduce the input space dimension, and therefore improve its sampling. In fact, the approach of logistic linear regression does not need to assume that the variables are independent, and the presence of covariance in the input data does not affect the quantification of the parameters of the optimal hyperplane separating high-z QSOs from the remaining classes except for causing a sampling of the input space lower than necessary. The good performance found for the test set of unseen data gives us confidence that although probably redundant, the selected set of input features is appropriate.

Several works described in the Introduction select QSOs from SDSS using colour and/or photometric information covering the five bands. Suchkov et al. (2005) apply a k-dimensional decision tree classifier and use five colours ($u - g, g - r, r - i, i - z$ and $g - i$) as input data. Gao et al. (2008) apply decision trees and support vector machines to select QSOs from a combined SDSS–2MASS sample, using several sets of input data including in all cases SDSS photometry at the five bands (magnitudes in all bands or four colours and a magnitude). They found the best results for the input set with four SDSS colours and the r-band magnitude, which is the set of optical data selected in our work. Ball et al. (2006, 2007) use decision trees to select QSOs from SDSS and a k nearest neighbour instance-based approach to quantify QSO photometric redshifts (Ball et al. 2008), in both cases using as input data four colours in the four magnitude types (PSF, fibre, Petrosian and model). Ball et al. (2007) applied genetic algorithms to investigate subsets of the original 16 inputs in a systematic way and found that no subset resulted in a significant improvement and some subsets were even worse, therefore, electing to keep the full SDSS information available.

Since we adopted the leave-one-out approach and use all the sources as test, training and testing objects form the same sample, i.e. the sample of sources with DR5 spectra. This means that the quoted figures of 96 ± 14 completeness and 62 ± 9 per cent efficiency refer to the selection of high-z QSOs among the labelled sources, i.e. within the interpolation regime.

The labelled sample contains, among the 52 high-z QSOs, 12 sources with broad absorption lines (BALs) or self-absorption at Lyα (see Table 2). The classifier recovers 50/52 of the high-z QSOs and 11/12 of the BALs and self-absorbed at Lyα, proving to be effective in the selection of QSOs with this type of absorption features. On the other hand, we confirmed that all 52 high-z QSOs in the training sample have at least an emission line with FWHM $\geq 1000\,{\rm km\,s^{-1}}$, i.e. none of them belongs to the class of 'narrow-lined' (type II) QSOs. Therefore, the classifier trained in this work targets the selection of high-z QSOs with at least a broad emission line, including those cases presenting absorption features in the form of BALs or Lyα absorption.

Fig. 5 shows the distribution of the six variables used as input data $r, u - g, g - r, r - i, i - z$ and radio–optical offset, separating (from left to right) labelled high-z QSOs, labelled non-high-z QSOs and unlabelled sources. For non-high-z QSOs (4196) and unlabelled sources (4415) we used for the plot representative subsets containing 8 per cent of the sources, to improve visualization. For non-high-z QSOs this proportion was applied separately for QSOs, galaxies, early-type stars, late-type stars and 'unknown', to keep the same fractions as in the original sample. Most of the sources in this sample are QSOs with $z < 3.6$ (3906/4248 = 90 per cent). The scale is linear, and although normalized variables were used, their ranges in physical units can be inferred from the marked numbers in the figure, showing the minimum and maximum value of each variable for the represented sources. Table 4 presents the mean, standard deviation and median for each variable, for the complete three samples, as well as for the whole sample of labelled sources. In Fig. 5 and Table 4 all sources were included regardless of their photometric errors. The errors at g, r, i and z are less than 0.2 mag (except for one unlabelled source with $\Delta r = 0.24$ and eight with $\Delta z = 0.2$–0.3). For the u band the errors exceed 0.2 mag for all high-z QSOs, 246 labelled non-high-z QSOs (out of 4196) and 313 unlabelled sources (out of 4415), with median values for these sources of $\Delta u = 0.8, 0.5, 0.4$, respectively.

Regarding the comparison among labelled sources, the variables that taken individually better discriminate between the classes of high-z QSOs and non-high-z QSOs are the $u - g$ and $g - r$ colours, as expected from the fact that $z < 3.6$ QSOs dominate the non-high-z QSO sample and the well established colour–redshift relation for QSOs (e.g. Schneider et al. 2007). Also noticeable is the concentration of high-z QSOs at the faintest r magnitudes (fainter magnitude and lower dispersion) and at the lowest radio–optical offsets (lower separation and again lower dispersion), compared to the remaining labelled sources.

4 APPLICATION OF THE NETWORK TO THE UNLABELLED SAMPLE

4.1 The labelled and unlabelled samples

The labelled sample consists of the FIRST–SDSS sources included in the DR5 spectroscopic catalogue. The content of the labelled

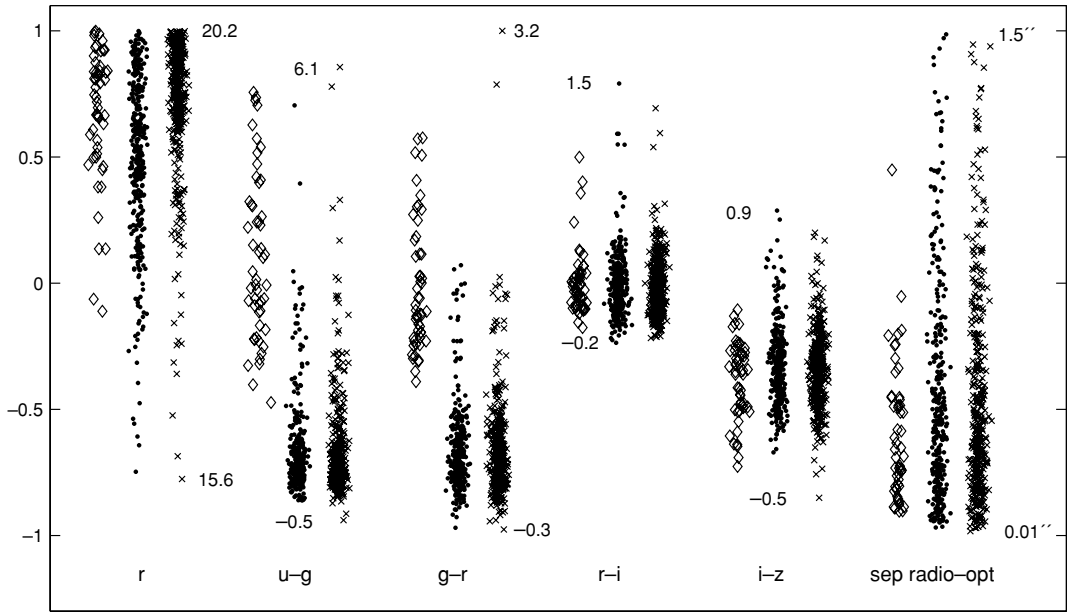

Figure 5. Normalized input parameters $r, u-g, g-r, r-i, i-z$ and radio–optical separation for labelled high-z QSOs (◇), labelled non-high-z QSOs (•, 8 per cent shown) and unlabelled sources (×, 8 per cent shown). The numbers indicate the minimum and maximum value of each variable (in magnitudes or arcsec) for the sources in the plot.

Table 4. Statistics (mean, standard deviation and median) of the selected input variables for various SDSS DR5 subsamples.

	High-z QSOs (52)	Non-high-z QSOs (4196)	Labelled (4248)	Unlabelled (4415)
r	19.36 ± 0.69	18.90 ± 0.86	18.90 ± 0.86	19.33 ± 0.81
	19.53	19.00	19.01	19.56
$u-g$	3.34 ± 1.20	0.54 ± 0.75	0.57 ± 0.82	0.53 ± 0.70
	3.07	0.31	0.32	0.32
$g-r$	1.40 ± 0.45	0.27 ± 0.31	0.29 ± 0.33	0.27 ± 0.30
	1.24	0.21	0.21	0.21
$r-i$	0.17 ± 0.22	0.16 ± 0.21	0.16 ± 0.22	0.15 ± 0.20
	0.13	0.14	0.14	0.13
$i-z$	0.06 ± 0.18	0.11 ± 0.17	0.11 ± 0.17	0.12 ± 0.18
	0.10	0.09	0.09	0.11
Sep (arcsec)	0.30 ± 0.20	0.40 ± 0.33	0.40 ± 0.33	0.39 ± 0.32
	0.25	0.29	0.29	0.28

sample is determined by the way the photometric objects were selected as spectroscopic targets by SDSS. The selection criteria were mainly aimed at obtaining samples of galaxies, QSOs and brown dwarfs, with different combinations of selected parameters (e.g. magnitude and colour ranges, extension, proximity to catalogued sources at other wavelengths) being used for each object type. The labelled sample cannot therefore be considered as statistically representative of the SDSS imaging data base. Classes not considered in the spectroscopic selection criteria may be absent or poorly represented in the spectroscopic catalogue. The unlabelled sample is therefore a mixture of the sources in the DR5 spectroscopic area not selected as spectroscopic targets (2059 objects within $\sim$5553 deg^2, compared to 4248 labelled in the same region), and the sources in the DR5 photometric area but outside the spectroscopic area (2356 objects within $\sim$1838 deg^2).

A general concern about classification is the application of an algorithm trained on a sample of data to a different set of data, likely covering other regions of input space. The extension of the classifier beyond the original sample used for the training is framed in the context of extrapolation versus interpolation. In our case the training set is the DR5 spectroscopic survey or labelled sample, and our aim is to apply the classifier to the sources in the DR5 photometric sample without DR5 spectra. We expect a reasonable overlap between labelled sources and the sources located outside the spectroscopic area, since a large fraction of the latter would have been SDSS spectroscopic targets if included in the spectroscopic area [a fraction $4248/(4248+2059) = 67$ per cent using the statistics in DR5 spectroscopic area]. A poorer overlap is expected between labelled sources and the unlabelled sources in DR5 spectroscopic area.

Fig. 5 and Table 4 allow to compare the distribution of each input variable for the classes of labelled and unlabelled sources. Although Fig. 5 does not include labelled sources as a whole, the distributions for this set are approximately similar to those for labelled non-high-z QSOs, since high-z QSOs make only 1.2 per cent (52/4248) of the labelled sources. The main effect of including high-z QSOs would be to increase the ranges of the $u-g$ and $g-r$ colours. The statistics of mean, standard deviation and median for the whole labelled and unlabelled groups are given in Table 4 (columns 3 and 4). Fig. 5 and Table 4 show a good agreement between the distributions of each of the input variables for unlabelled and labelled sources, except for the r-band magnitudes, which are fainter for unlabelled sources, with mean and median of 19.33 and 19.56 versus 18.90 and 19.01. These comparisons between unlabelled and labelled sources use each input variable individually. More complex separations between labelled and unlabelled sources would be expected in the six-dimensional input space.

We applied the trained classifier to the unlabelled sample in order to select new high-z QSO candidates and to obtain an estimate of the completeness of SDSS spectroscopy for radio QSOs with $3.6 \leq z \leq 4.6$. The sample of new high-z QSO candidates is presented in Section 4.2. In Section 4.3 we discuss the performance obtained in the unlabelled sample, on the basis of available

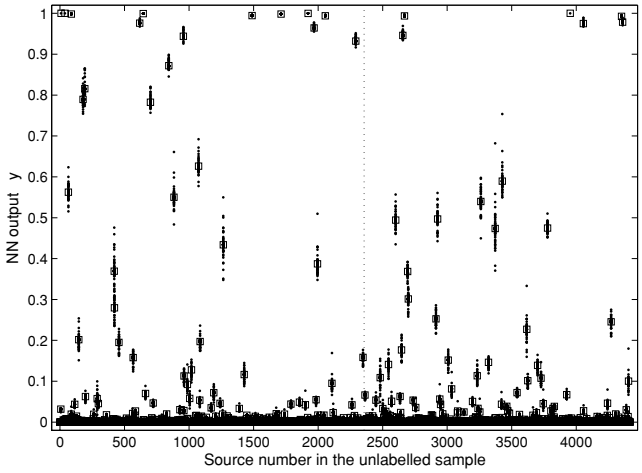

Figure 6. Distribution of NN output y for the unlabelled FIRST–DR5 sources and the separation high-z QSO versus remaining classes, assuming the trained NNs (see Section 4.2). The boxes mark the median values. The sources to the left of the vertical line (2356) are located outside the DR5 spectroscopic area, and those to right (2059) inside this area.

spectroscopic identifications from observations in this work, taken from the literature or from SDSS DR6.

4.2 The sample of high-z QSO candidates

In Section 3 we demonstrated the good performance of simple NNs for separating, on the basis of optical photometry and radio data, high-z QSOs from the remaining classes in the labelled sample. This evaluation was based on the outputs of $m = 4248$ labelled objects, using for each object a NN trained with the remaining 4247. We adopted set B of input variables, which for threshold $y_c = 0.1$ yielded completeness 96 ± 14 per cent and efficiency 62 ± 9 per cent. The m NNs were applied to the unlabelled sample and the resulting m values of y for each source, and their medians, y_{med}, are shown in Fig. 6. The number of unlabelled sources with median outputs exceeding $y_c = 0.1$ is 58 (31 outside and 27 within the DR5 spectroscopic area), and these are our 'high-z QSO candidates'. Their properties are listed in Table 5, including the median of the NN outputs. The same parameter for the high-z QSOs in the labelled sample is listed in Table 2 (but in this case the QSOs themselves were used in the training).

4.3 Spectroscopic check of the QSO selection

The quality of the selection of high-z QSO candidates was tested by comparison with spectroscopy from the NED, from a dedicated observing programme with Intermediate-dispersion Spectrograph and Imaging System (ISIS) at the WHT, and from spectroscopic classifications from SDSS DR6. The resulting classifications and redshifts are included in Table 5.

4.3.1 Spectroscopic classifications from NED

Counterparts of the 58 high-z QSO candidates and the 4357 non-candidates (4415 unlabelled sources) were sought in NED in 2007 February, using a search radius of 5 arcsec. A similar radius is used in the SDSS DR5 Quasar Catalog (Schneider et al. 2007) to quote the association with a NED object. Four of the candidates were spectroscopically classified, all QSOs with $z > 3.3$. Benn et al. (2002) identified three of them, with redshifts 4.33, 4.17 and 3.694, the remaining candidate, with $z = 3.305$, was identified by Mason et al. (2000).

Amongst the non-candidates, 382 were associated with QSOs (blazars excluded) with secure redshifts, and none of them had $z \geq 3.6$. Another 13 QSOs had ambiguous or uncertain redshifts but none was consistent with $z \geq 3.6$.

4.3.2 Spectroscopy with ISIS

Spectra of 27 of the remaining 54 candidates were obtained with the WHT's ISIS dual-arm spectrograph in two runs on 2007 April 3, 4, 6 and 7 and on 2007 July 8, 9 and 10. The R158R grating was used on the red arm, yielding a wavelength range 5300–10000 Å with dispersion 1.8 Å pixel^{-1}. On the blue arm the R300B grating was used, giving a spectral range 3000–6000 Å with dispersion 0.9 Å pixel^{-1}. Exposure times were 600 s. Spectrophotometric standard stars were observed in order to calibrate the instrumental spectral response. Seeing was typically better than 1 arcsec and the slit width was set to 1 arcsec, yielding spectral resolution, as measured from sky lines, of 7.7 and 4.5 Å in the red and blue arms, respectively. Standard data reduction was carried out using the IRAF[3] package. Arc-lamp exposures were used for wavelength calibration, giving solutions with residuals <0.1 Å.

We observed 15 sources in April, prioritizing the candidates with higher NN output y, brighter r magnitude and at lower air mass, regardless of their location inside or outside the DR5 spectroscopic area. All 15 sources were classified as QSOs and their redshifts were determined as the average of the values measured from individual emission-line centroids, usually Lyα, Si IV and C IV. 13 of the QSOs have $3.60 \leq z \leq 4.21$, and the remaining two $z = 3.55$ and 3.42.

The 12 sources observed in July consist of *all* the remaining candidates with RA in the range 13–24 h and without spectra in DR6. The results of the spectroscopic classification were as follows. 11 sources were classified as QSOs: four with $3.6 \leq z \leq 3.9$, four with $1.07 \leq z \leq 1.34$ and three with $z = 3.17$, 3.34 and 3.59. One candidate remained unclassified due to both low signal-to-noise ratio and lack of clear absorption or emission features in the spectrum.

Fig. 7 shows the spectra of the 21 candidates identified with ISIS as $z \geq 3.2$ QSOs (17 of them with $z \geq 3.6$).

4.3.3 Spectroscopy from SDSS DR6

SDSS DR6 (CAS SpecObj view) includes spectra of nine of the remaining 27 candidates (and also of six of those already observed with ISIS in April, and two from the NED). These nine include four QSOs with $3.6 \leq z \leq 3.8$, one at $z = 3.40$, two galaxies with $z = 0.45$ and 0.58 and two sources labelled as unknown.

Amongst the 4357 non-candidates, 898 have spectra from DR6, and are classified as stars or galaxies (71), unknown (62) or QSOs (765). The latter include some of the QSOs with spectra from NED cited in Section 4.3.1. Two QSOs have $z \geq 3.6$, but their SDSS redshifts are incorrect (see the DR6 spectra in Fig. 8). For SDSS 075558.88+113210.9, with quoted $z = 4.340$ (confidence = 0.51), we measured from the emission lines of Mg II

[3] IRAF is distributed by the National Optical Astronomy Observatories, which is operated by Association of Universities for Research in Astronomy, Inc., under cooperative agreement with the National Science Foundation.

Table 5. $z \geq 3.6$ QSO candidates identified by the NN in the FIRST–SDSS DR5 unlabelled sample.

RA (J2000) (1)	Dec. (J2000) (2)	r_{AB} (3)	$S_{1.4\,GHz}$ (mJy) (4)	NN output y_{med} (5)	Redshift NED	Redshift WHT (6)	Redshift DR6	Notes (7)	In DR6 spec. area? (8)
07 25 18.26	37 05 18.3	19.61	26.56	1.00	4.33				
07 47 11.15	27 39 03.3	18.35	1.55	0.11	4.17				Yes
07 47 38.49	13 37 47.3	19.37	6.62	1.00		4.04		BAL	
08 07 10.74	13 17 39.4	20.01	48.88	0.56		3.70	3.726		Yes
08 15 55.01	46 53 21.4	19.88	3.73	0.14					Yes
08 23 23.32	15 52 06.8	19.31	79.33	1.00		3.79	3.781		Yes
08 33 16.91	29 22 28.0	20.13	12.73	0.49					Yes
08 43 23.69	16 56 56.1	19.66	2.36	0.20				DR6 unknown	Yes
08 48 18.88	39 38 06.0	20.15	0.72	0.18					Yes
08 52 58.87	22 50 50.5	20.16	45.33	0.95		3.55			Yes
08 55 01.82	18 24 37.8	19.96	9.43	0.79		3.96	3.966		Yes
08 59 44.06	21 25 11.1	18.72	23.96	0.82		3.70	3.699		Yes
09 02 54.17	41 35 06.5	20.12	0.93	0.99		3.69			Yes
09 09 53.84	47 49 43.0	19.89	383.67	0.37					Yes
09 14 36.22	50 38 48.5	20.16	51.00	0.30					Yes
10 09 33.22	25 59 01.2	20.13	3.42	0.37				DR6 unknown	Yes
10 10 20.85	28 51 50.1	20.11	2.62	0.28				DR6 $z = 0.58$ galaxy	Yes
10 19 39.00	19 03 12.0	20.11	0.74	0.20				DR6 $z = 0.45$ galaxy	Yes
10 29 40.93	10 04 10.9	19.47	3.22	0.25					Yes
10 34 20.43	41 49 37.5	20.12	1.98	0.50					Yes
10 52 25.06	25 15 41.3	20.10	5.26	0.16			3.404		Yes
10 58 07.47	03 30 59.6	19.92	4.62	0.15					Yes
11 05 43.86	25 53 43.1	20.09	2.76	0.98			3.779		Yes
11 09 46.44	19 02 57.6	20.04	6.95	1.00					
11 23 39.59	29 17 10.7	19.47	3.14	0.78			3.771		Yes
11 46 41.02	12 52 02.9	20.19	3.01	0.11					Yes
11 51 07.42	50 15 58.5	20.08	1.22	0.54					Yes
11 54 49.36	18 02 04.4	19.63	39.06	0.87			3.688		Yes
12 04 07.83	48 45 48.2	19.97	2.64	0.15					Yes
12 05 31.73	29 01 49.2	20.17	1.46	0.55					Yes
12 13 29.42	−03 27 25.7	19.64	25.53	0.47					Yes
12 20 27.96	26 19 03.5	18.12	35.04	0.94	3.694		3.697		Yes
12 21 35.64	28 06 13.8	19.77	28.76	0.11	3.305		3.288		Yes
12 28 19.96	47 40 30.4	19.32	2.22	0.59					Yes
12 31 28.22	18 47 14.3	19.41	11.17	0.13					
12 43 23.16	23 58 42.2	19.87	63.44	0.63					
12 44 43.06	06 09 34.6	19.78	1.36	0.20					Yes
13 12 42.86	08 41 05.0	18.53	3.93	0.43		3.73	3.743		Yes
13 20 53.63	10 37 51.5	19.46	8.43	0.23		3.42	3.431		Yes
13 22 27.58	53 52 09.2	19.68	2.51	0.10		1.23			Yes
13 37 59.43	36 34 20.6	20.17	2.88	0.12		1.07			Yes
13 42 01.42	05 01 56.0	20.11	27.24	0.14		3.17			Yes
13 48 54.37	17 11 49.6	19.13	1.90	0.99		3.60			
13 49 18.52	35 24 15.7	19.77	81.88	0.11		1.22			Yes
14 06 35.67	62 25 43.3	19.72	11.50	0.47		3.89		abs	Yes
14 34 13.05	16 28 52.7	19.86	4.95	1.00		4.21			
14 53 29.01	48 17 24.9	20.11	3.75	1.00		3.77			Yes
15 11 46.99	25 24 24.3	19.95	1.39	1.00			3.719	BAL	Yes
15 20 28.14	18 35 56.1	19.82	6.94	0.96		4.11			
15 24 24.35	07 31 29.9	20.13	1.51	0.39		3.59			Yes
15 33 36.14	05 43 56.5	19.84	28.29	0.99		3.93			
15 37 56.90	48 23 32.3	20.00	3.07	0.97		1.34			Yes
16 37 08.29	09 14 24.6	19.56	9.43	0.93		3.75			
17 02 53.54	23 57 58.0	19.74	19.24	0.25				Unknown	Yes
17 20 02.17	24 55 48.8	19.82	12.90	0.16		3.34		BAL	
22 28 14.39	−08 55 25.7	20.19	1.99	0.99		3.64			Yes
22 35 35.59	00 36 02.0	20.14	4.32	0.98		3.87			Yes
23 50 22.39	−09 51 44.3	19.68	6.51	0.10		3.70			Yes

The columns give the following: (1, 2, 3, 4) similar to Table 2; (5) NN output (see Section 4.2); (6) redshifts from NED (SDSS 072518.26+370518.3, SDSS 074711.15+273903.3 and SDSS 122027.96+261903.5 from Benn et al. 2002; SDSS 122135.64+280613.8 from Mason et al. 2000), from this work or from DR6; (7) BAL – broad absorption line QSO; abs – the Lyα line appears to be self-absorbed; (8) indicates the sources located within the spectroscopic plates available in DR6.

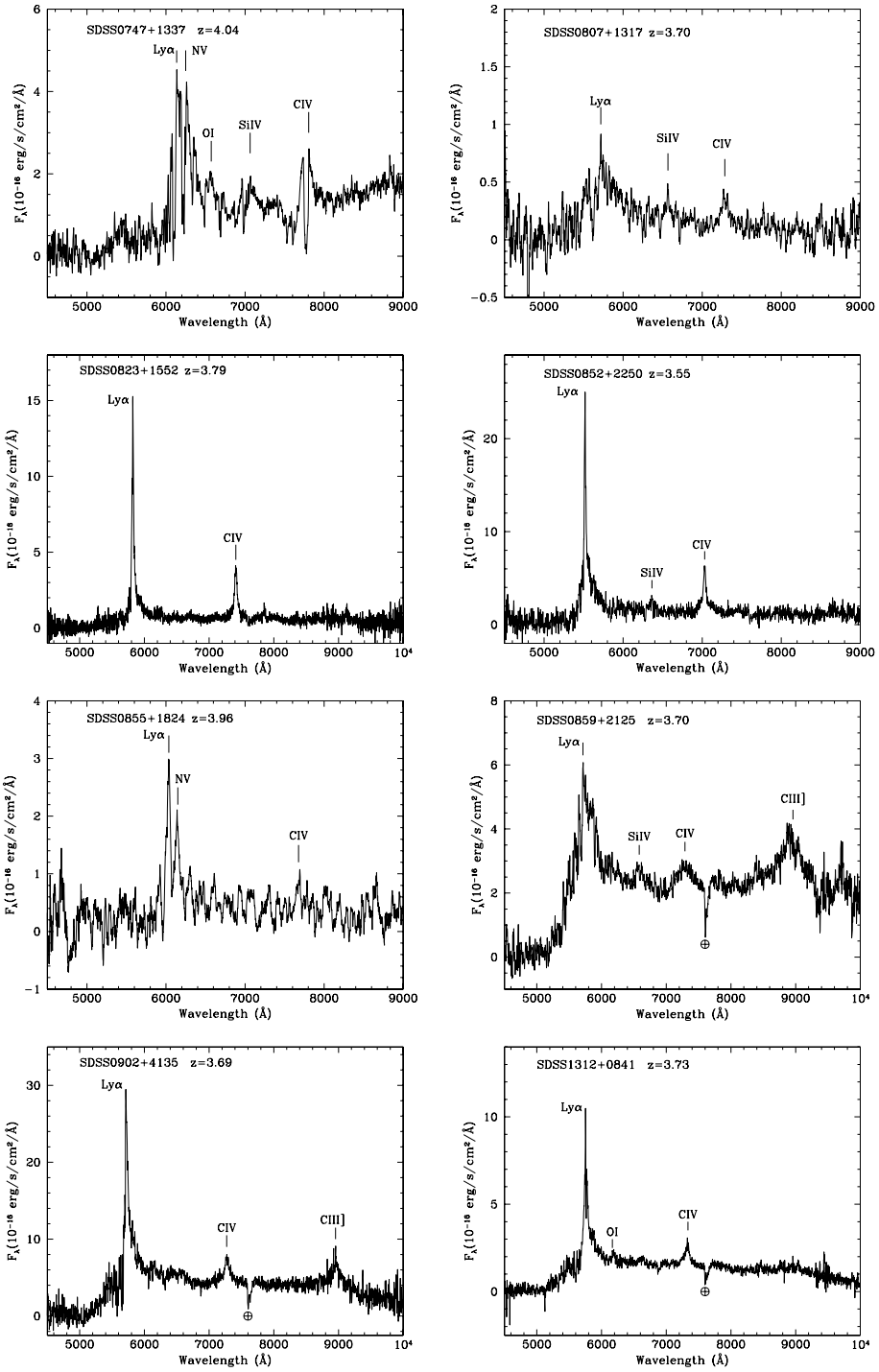

Figure 7. WHT spectra of 21 of the 58 NN $y_{\rm med} \geq 0.1$ candidates (six also included in DR6), including 17 $z \geq 3.6$ QSOs, and four QSOs at $z = 3.34$, 3.42, 3.55 and 3.59. Emission features are labelled by ion. Symbol $\oplus$ indicates the position of the atmospheric absorption band O_2 A.

(erroneously taken as Lyα by the SDSS pipelines) and C III] a redshift $z = 1.295$. The spectrum of SDSS 161836.09+153313.5, with $z = 4.376$ (confidence = 0.00), resembles that found for sources SDSS 130941.36+112540.1 and SDSS 153420.23+413007.5 (see Section 2), classified in DR5 as QSOs with redshifts $z = 4.395$ and 4.426, but with revised values in DR5Q $z = 1.362$ and 1.400, due to the re-interpretation of the assumed Lyα emission line as Mg II. A similar revision gives $z = 1.322$ for SDSS 161836.09+153313.5.

4.3.4 Performance of the selection of high-redshift QSOs

Spectra are available for 40 candidates, obtained from NED, SDSS DR6 or observed for this work, and 24 of them are confirmed $z \geq 3.6$ QSOs.

Fig. 9 shows a plot of the NN output $y_{\rm med}$ versus r magnitude for the 58 high-z QSO candidates. Different symbols correspond to the different spectral classes (high-z QSOs are shown as diamonds). The two panels separate the candidates located within and outside

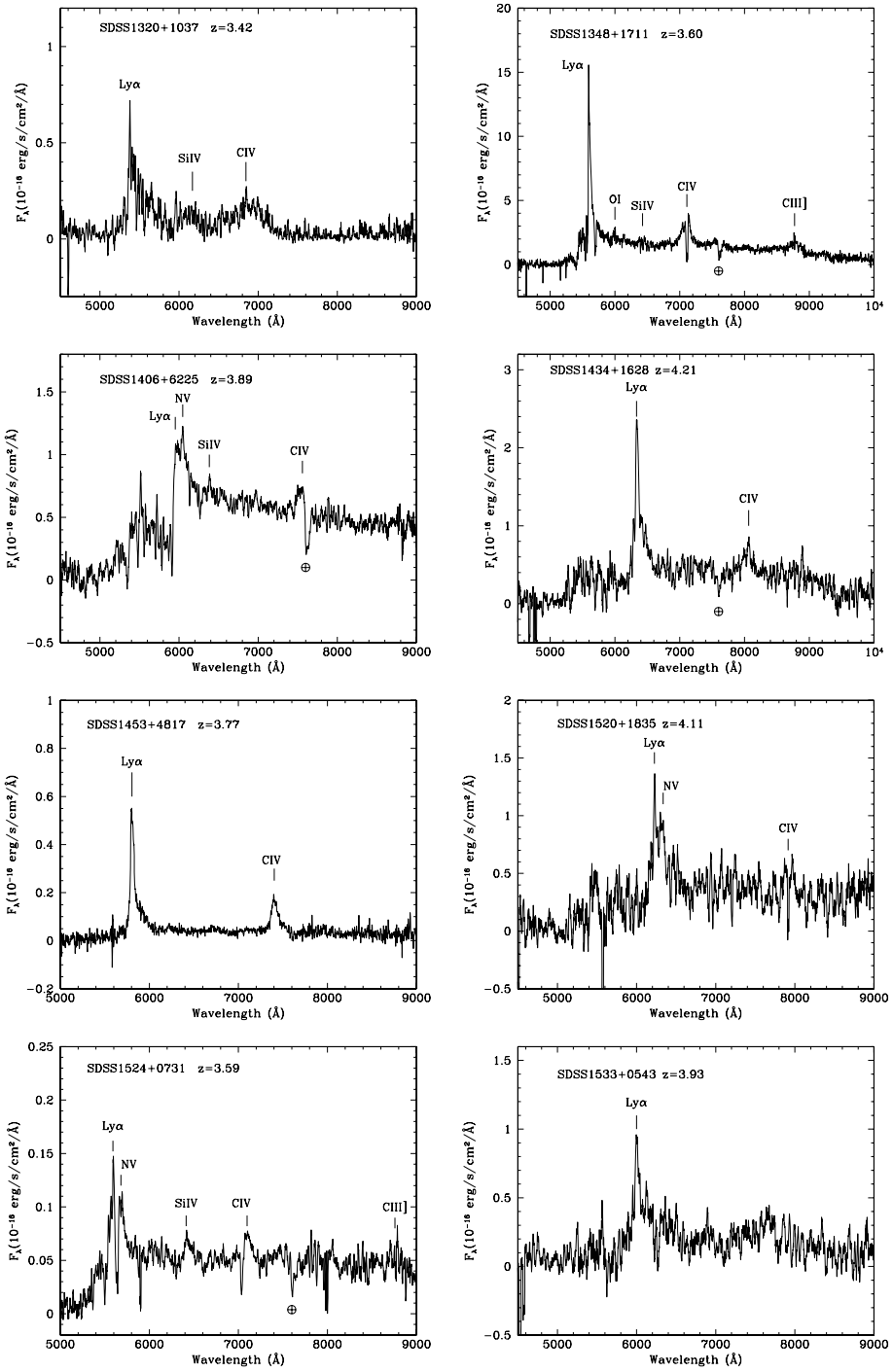

Figure 7 – *Continued*

the spectroscopic area available in DR6 (as noted in the last column of Table 5). Fig. 9 shows a larger fraction of high-z QSOs among the candidates with higher NN outputs, a trend also evident in Fig. 2. The efficiency for $0.55 \leq y \leq 1$ is 91 per cent (20 $z \geq 3.6$ QSOs out of 22 candidates with available spectra), dropping to 22 per cent (four of 18) for $0.1 \leq y < 0.55$. Spectra are available for all 20 high-z QSO candidates with $13^{\rm h} < {\rm RA} < 24^{\rm h}$, and this set therefore forms a complete subsample with regard to the distribution of NN outputs. With 12 confirmed $z \geq 3.6$ QSOs out of 20 candidates, the efficiency from this sample is 60 ± 17 per cent. This value is in good agreement with the efficiency $24/40 = 60 \pm 12$ per cent for the total sample of candidates with spectra, and with the 62 ± 9 per cent efficiency obtained within the labelled sample (Section 3).

None of the non-candidates in the unlabelled sample with available spectrum from NED or DR6 is a $z \geq 3.6$ QSO, therefore, we have no evidence of incompleteness, with respect to DR5 unlabelled sources with matches in any of these data bases. In fact a good completeness was expected for the matches with the DR6 spectroscopic survey, since the selection of sources, classification and measured properties respond to the same scheme as for the DR5 spectroscopic catalogue used for the training, where we had found

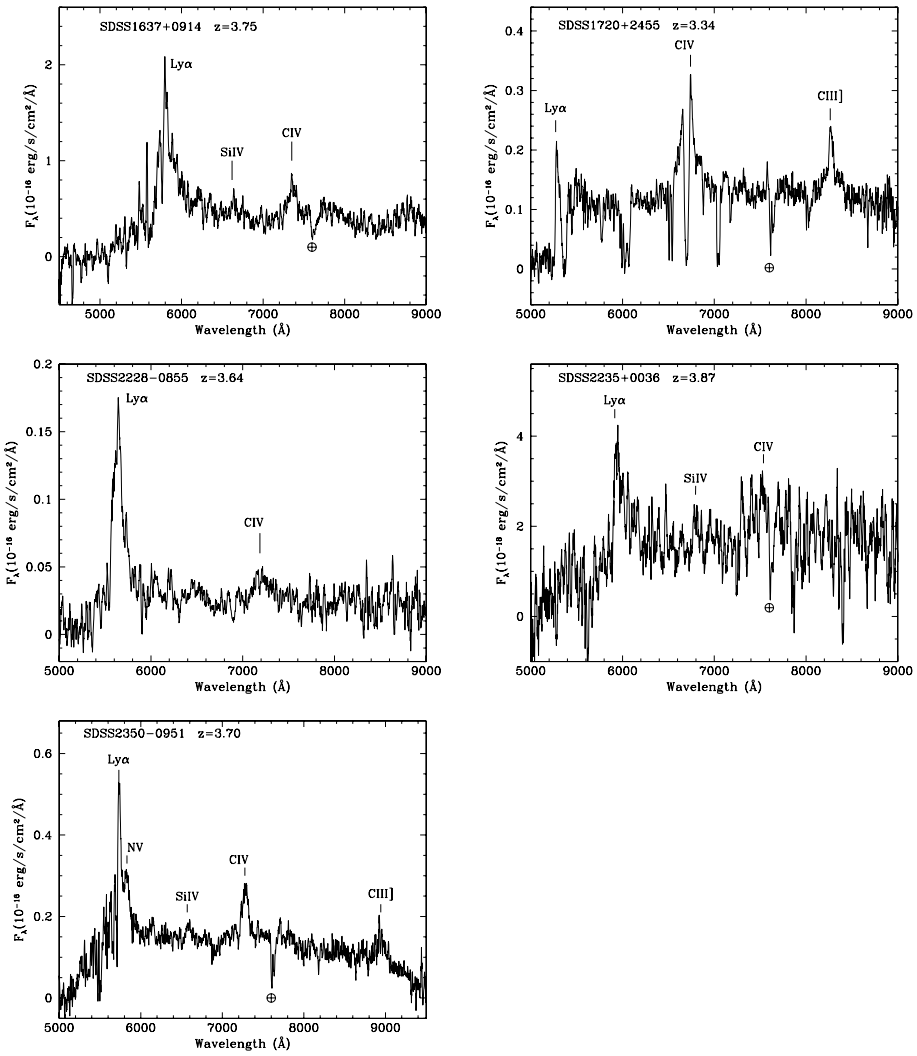

Figure 7 – *Continued*

96 per cent completeness. However, the NED provides spectroscopic identifications assigned from other surveys, and the absence of NED high-z QSOs among the non-candidates gives therefore independent evidence that the classifier has a good completeness in its extension to DR5 unlabelled sources. Three DR5 unlabelled sources are identified as $z \geq 3.6$ QSOs in NED, all of them selected as high-z QSO candidates in our work.

5 DISCUSSION AND CONCLUSIONS

In this paper we aimed to obtain a sample of $z \geq 3.6$ QSOs, starting from an initial complete sample of 8665 FIRST sources with star-like counterparts in the SDSS DR5 photometric survey, of which 4250 have spectra in DR5, 52 of them being $z \geq 3.6$ QSOs. We found that simple supervised NNs, trained on the sources with DR5 spectra, and using optical photometry and radio data as input parameters, allow separation of high-z QSOs from the remaining spectral classes with 96 per cent completeness and 62 per cent efficiency. The application of the NNs to the sample of 4415 sources without DR5 spectra yielded 58 high-z QSO candidates.

We obtained spectra of 27 of the 58 candidates, and 17 were confirmed as high-z QSOs. Spectra of 13 additional candidates from the NED and from DR6 revealed seven more high-z QSOs, yielding a total 40 candidates with spectra available, of which 24 are high-z QSOs. The number of high-z QSOs was then increased from 52 in the initial sample to 76 (a factor of 1.46).

The overall efficiency in the selection of new high-z QSOs is 60 ± 12 per cent (24/40). The estimate from a subsample unbiased with respect to the NN outputs is 60 ± 17 per cent (12/20), and both values are in good agreement with the 62 ± 9 per cent efficiency obtained for the DR5 labelled sample (Section 3).

None of the non-candidates with spectra available from NED or DR6 is a $z \geq 3.6$ QSO, therefore, we have no evidence of incompleteness regarding high-z QSOs with matches in these catalogues. Since the NED spectroscopic identifications are assigned from a variety of surveys different than SDSS, the database provides a blind test of the good completeness of the classifier for DR5 unlabelled sources.

The efficiencies found are well above the values obtained for previous samples of RL high-z QSOs, based on less accurate optical photometry and with fewer wavelength bands than SDSS, although already highly complete ($\geq$95 per cent) regarding optical colour selection. The efficiencies for various samples, summarized by Carballo et al. (2006) for $z \geq 3.7$, are 12–13 per cent (Holt et al.

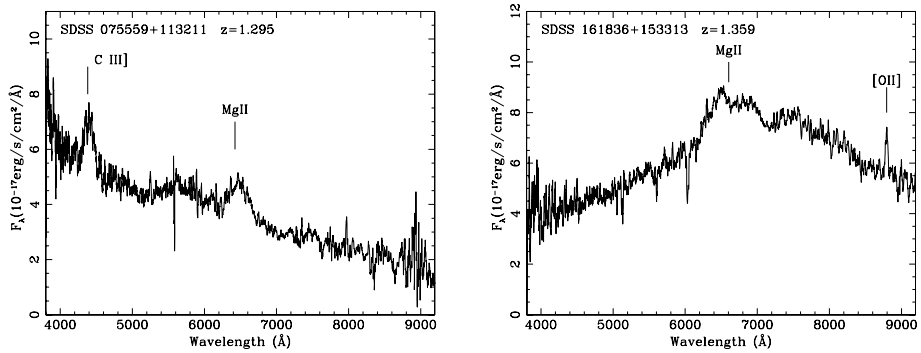

Figure 8. DR6 spectra of two non-candidates with revised redshifts $z = 1.29$ and 1.32 listed in SDSS DR6 as $z \geq 3.6$ QSOs, due to misidentification between the Lyα and Mg II emission lines.

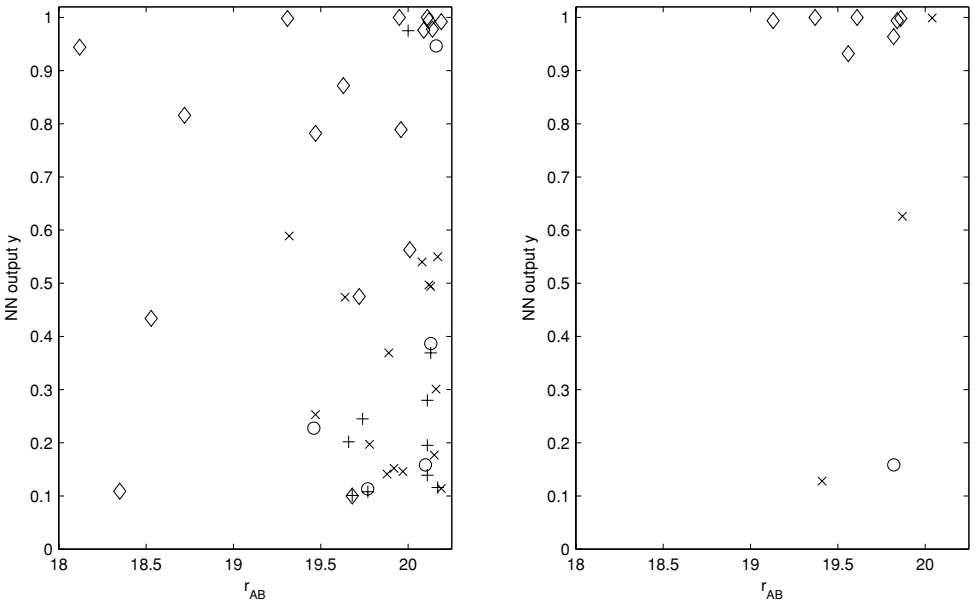

Figure 9. NN output y versus r magnitude for the 58 high-z QSO candidates, located either within (left-hand panel) or outside (right-hand panel) the spectroscopic area available in DR6. $\diamond$: QSOs with $z \geq 3.6$; $\circ$: QSOs with $3.2 \leq z < 3.6$; $+$: other classification or unknown; $\times$: without spectrum.

2004; Carballo et al. 2006; $S_{1.4\,\mathrm{GHz}} > 1$ mJy, APM-POSS E, O), 6 per cent (Hook et al. 2002; $S_{5\,\mathrm{GHz}} > 30$ mJy and radio flat, APM-POSS E, O) and 19 per cent (Snellen et al. 2001; $S_{5\,\mathrm{GHz}} > 30$ mJy and radio flat, APM UKST (United Kingdom Schmidt Telescope) B, R, I).

Adopting for the 18 candidates which still lack spectroscopy a weighted efficiency of 37 per cent (four candidates with $y \geq 0.55$ and 14 with $y < 0.55$, with expected efficiencies of 91 and 22 per cent, respectively), we calculate ∼seven additional $z \geq 3.6$ QSOs. The FIRST–DR5 sample of high-z QSOs is thus expected to contain ∼83 QSOs (52+24+7). Adopting as a lower limit for completeness the nominal value of 96 per cent found for the labelled sample, we calculate for the set of 31 high-z QSOs obtained by the classifier (24 discovered and seven predicted) a minimum ∼one missed high-z QSO.

The NNs found 31 contaminants, i.e. non-high-z QSOs erroneously selected as high-z QSOs, in the labelled sample, with a fraction 61 ± 14 per cent (19/31) being QSOs with $3.2 \leq z \leq 3.6$. Among the 40 high-z QSO candidates with available spectra we found 16 contaminants, seven of them being QSOs with $3.15 \leq z \leq 3.6$, confirming a high rate of QSOs with z near the threshold $z = 3.6$ among the contaminants, $7/16 = 44 \pm 17$ per cent.

Our results allow us to obtain an estimate of the incompleteness of SDSS for the spectroscopic classification of FIRST high-z QSOs. 47 of the high-z QSO candidates are located in the spectroscopic area covered by DR6 (Table 5, Fig. 9, left-hand panel), and 17 of them are $z \geq 3.6$ QSOs, 10 included in the DR6 spectroscopic catalogue and seven not included. 15 candidates in this area still lack spectroscopy, and assuming for them a weighted efficiency of 31 per cent (two candidates with $y \geq 0.55$ and 13 with $y < 0.55$), we expect another four high-z QSOs. From this calculation we estimate 11 FIRST high-z QSOs missed by SDSS (seven QSOs and four candidates), which when compared to 62 (52+10) identifications yields an incompleteness of SDSS for the spectroscopic classification of FIRST $3.6 \leq z \leq 4.6$ QSOs of ∼15 per cent (11/73) for $r \leq 20.2$.

The definition of the original sample of 52 high-z FIRST QSOs excluded lobe-dominated morphologies and 'narrow-lined' QSOs, and included QSOs with BALs or self-absorbed at Lyα. The same conditions hold for the larger sample of 76 QSOs, obtained from the application of the NNs trained using these 52 objects to DR5

photometric sources without spectra in DR5, and covering a slightly wider region of input space than that used by SDSS for QSO targeting.

In a future paper we plan to analyse the optical luminosity function of FIRST–SDSS QSOs at $3.6 \leq z \leq 4.6$ on the basis of this sample. Concurrently we expect to carry out spectroscopic observations of the 18 candidates without spectra. Given the efficacy of our approach, we intend to extend the sample using more updated SDSS data releases, increasing the number of training sources and the number of high-z QSO candidates, for which subsequent spectroscopy will be planned. We envisage using additional infrared data via UKIRT (United Kingdom Infrared Telescope) Infrared Deep Sky Survey (UKIDSS).

ACKNOWLEDGMENTS

We are grateful to the referee for a prompt and useful report, which improved the paper. RC, JIG-S, CRB and FJ-L acknowledge financial support from the Spanish Ministerio de Educación y Ciencia under project AYA 2005-00055. We acknowledge the Isaac Newton Group's (ING) service programme for a generous allocation of observing time for this project and we thank ING staff for carrying out the observations.

Funding for the creation and distribution of the SDSS Archive has been provided by the Alfred P. Sloan Foundation, the Participating Institutions, the National Aeronautics and Space Administration, the National Science Foundation, the US Department of Energy, the Japanese Monbukagakusho and the Max Planck Society. The SDSS Web site is http://www.sdss.org/. The SDSS is managed by the Astrophysical Research Consortium (ARC) for the Participating Institutions. The Participating Institutions are the University of Chicago, Fermilab, the Institute for Advanced Study, the Japan Participation Group, the Johns Hopkins University, the Korean Scientist Group, Los Alamos National Laboratory, the Max-Planck-Institute for Astronomy (MPIA), the Max-Planck-Institute for Astrophysics (MPA), New Mexico State University, University of Pittsburgh, University of Portsmouth, Princeton University, the United States Naval Observatory and the University of Washington. This research has made use of the NED which is operated by the Jet Propulsion Laboratory, California Institute of Technology, under contract with the National Aeronautics and Space Administration.

REFERENCES

Adelman-McCarthy J. et al., 2007, ApJS, 172, 634
Bailer-Jones C. A. L., Irwin M., von Hippel T., 1998, MNRAS, 298, 361
Ball N. M., Loveday J., Fukugita M., Nakamura O., Okamura S., Brinkmann J., Brunner R. J., 2004, MNRAS, 348, 1038
Ball N. M., Brunner R. J., Myers A. D., Tcheng D., 2006, ApJ, 650, 497
Ball N. M., Brunner R. J., Myers A. D., Strand N. E., Alberts S. L., Tcheng D., Llorà X., 2007, ApJ, 663, 774
Ball N. M., Brunner R. J., Myers A. D., Strand N. E., Alberts S. L., Tcheng D., 2008, ApJ, 683, 12
Bazell D., Miller D. J., SubbaRao M., 2006, ApJ, 649, 678
Becker R. H., White R. L., Helfand D. J., 1995, ApJ, 450, 559
Benn C. R., Vigotti M., Pedani M., Holt J., Mack K.-H., Curran R., Sánchez S. F., 2002, MNRAS, 329, 221
Bertin E., Arnouts S., 1996, A&AS, 117, 393
Bishop C. M., 1995, Neural Networks for Pattern Recognition. Oxford Univ. Press, Oxford
Carballo R., Cofiño A. S., González-Serrano J. I., 2004, MNRAS, 353, 211
Carballo R., González-Serrano J. I., Montenegro-Montes F. M., Benn C. R., Mack K.-H., Pedani M., Vigotti M., 2006, MNRAS, 370, 1034
Cirasuolo M., Magliocchetti M., Gentile G., Celotti A., Cristiani S., Danese L., 2006, MNRAS, 371, 695
Claeskens J.-F., Smette A., Vandenbulcke L., Surdej J., 2006, MNRAS, 367, 879
Collister A. A., Lahav O., 2004, PASP, 116, 345
Crom S. M., Smith R. J., Boyle B. J., Shanks T., Miller L., Outram P. J., Loaring N. S., 2004, MNRAS, 349, 1397
Cutri R. M. et al., 2003, The IRSA 2MASS All-Sky Point Source Catalog. NASA/IPAC Infrared Science Archive
de Vries W. H., Becker R. H., White R. L., 2006, AJ, 131, 666
Firth A. E., Lahav O., Somerville R. S., 2003, MNRAS, 339, 1195
Folkes S. R., Lahav O., Maddox S. J., 1996, MNRAS, 283, 651
Gao D., Zhang Y.-X., Zhao Y.-H., 2008, MNRAS, 386, 1417
Hagan M. T., Menhaj M., 1994, IEEE Trans. Neural Netw., 5, 989
Holt J., Benn C. R., Vigotti M., Pedani M., Carballo R., González-Serrano J. I., Mack K.-H., Garcá B., 2004, MNRAS, 348, 857
Hook I. M., McMahon R. G., Shaver P. A., Snellen I. A. G., 2002, A&A, 391, 509
Ivezic Z. et al., 2004, in Richards G. T., Hall P. B., eds, ASP Conf. Ser. Vol. 311, AGN Physics with the Sloan Digital Sky Survey. Astron. Soc. Pac., San Francisco, p. 347
Jiang L., Fan X., Ivezic Z., Richards G. T., Schneider D. P., Strauss M. A., Kelly B. C., 2007, ApJ, 656, 680
Kormendy J., Richstone D., 1995, ARA&A, 33, 581
Lahav O., Naim A., Sodré L. Jr, Storrie-Lombardi M. C., 1996, MNRAS, 283, 207
Magorrian J. et al., 1998, AJ, 115, 2285
Mason K. O. et al., 2000, MNRAS, 311, 456
Richards G. T. et al., 2002, AJ, 123, 2945
Richards G. T. et al., 2004, ApJS, 155, 257
Richards G. T. et al., 2006, AJ, 131, 2766
Rohde D. J., Drinkwater M. J., Gallagher M. R., Downs T., Doyle M. T., 2005, MNRAS, 360, 69
Schlegel D. J., Finkbeiner D. P., Davis M., 1998, ApJ, 500, 525
Schneider D. P. et al., 2007, AJ, 134, 102
Snellen I. A. G., McMahon R. G., Dennett-Thorpe J., Jackson N., Mack K.-H., Xanthopoulos E., 2001, MNRAS, 325, 1167
Suchkov A. A., Hanisch R. J., Margon B., 2005, AJ, 130, 2439
Vigotti M., Carballo R., Benn C. R., de Zotti G., Fanti R., González-Serrano J. I., Mack K.-H., Holt J., 2003, ApJ, 591, 43
Voges W. et al., 1999, A&A, 349, 389
Voges W. et al., 2000, Int. Astron. Union Circ., 7432, 3
Weinstein M. A. et al., 2004, ApJS, 155, 243
York D. G. et al., 2000, AJ, 120, 1579

This paper has been typeset from a TEX/LATEX file prepared by the author.